JACS
JOURNAL OF THE AMERICAN CHEMICAL SOCIETY

Article

pubs.acs.org/JACS

A Role for Pd(IV) in Catalytic Enantioselective C–H Functionalization with Monoprotected Amino Acid Ligands under Mild Conditions

R. Erik Plata,[†] David E. Hill,[†] Brandon E. Haines,[‡] Djamaladdin G. Musaev,[‡] Ling Chu,[†] David P. Hickey,[§] Matthew S. Sigman,[§] Jin-Quan Yu,[†] and Donna G. Blackmond*[,†]

[†]Department of Chemistry, The Scripps Research Institute, La Jolla, California 92037, United States
[‡]Cherry L. Emerson Center for Scientific Computation, Emory University, Atlanta, Georgia 30322, United States
[§]Department of Chemistry, University of Utah, Salt Lake City, Utah 84112, United States

Supporting Information

ABSTRACT: Kinetic and mechanistic studies of the desymmetrization of benzhydrylamine using Pd/monoprotected amino acid ligands (Pd/MPAA) via C–H functionalization with molecular iodine provide mechanistic insight into the rate-determining step and the oxidation state of Pd in the C–H functionalization step. Enantiomeric excess is strikingly insensitive to temperature from ambient temperature up to over 70 °C, and reaction rate is insensitive to the electronic characteristics of the ligand's benzoyl protecting group. The reaction is highly robust with no evidence of catalyst deactivation. Intriguingly, C–H bond breaking does not occur prior to the addition of I_2 to the reaction mixture. Electrochemical experiments demonstrate the viability of oxidative addition of I_2 to Pd(II). Together with ^{19}F NMR studies, these observations suggest that iodine oxidizes Pd prior to addition of the amine substrate. This work may lead to a better general understanding of the subtle variations in the reaction mechanisms for C–H functionalization reactions that may be extant for this ligand class depending on substrate, amino acid ligand and protecting group, and reaction conditions.

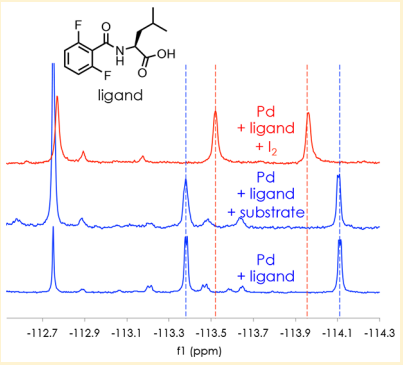

INTRODUCTION

C–H activation reactions employing broadly useful substrates and the concept of weak coordination have gained attention in recent years.[1] In particular, triflyl-protected diarylamines have demonstrated a broad scope as substrates in enantioselective iodination via both desymmetrization (Scheme 1)[2] and kinetic resolution.[3] Those reports followed the finding that a weakly coordinating amide auxiliary could effect the *ortho*-iodination of benzamides using I_2 as the sole oxidant.[4] The mild conditions of these reactions stand out in comparison to many of the other reactions employing monoprotected amino acid (MPAA) ligands, prompting us to study the reaction in Scheme 1 in detail to probe for deeper understanding. The present investigation reports mechanistic studies that suggest a novel role for Pd(IV) in the C–H activation process. This finding should enable further development of similar reactions.

Scheme 1. Iodination of Diarylmethylamines

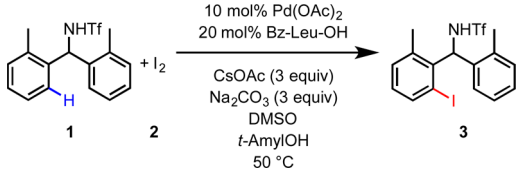

RESULTS AND DISCUSSION

Because optimization studies identified the leucine amino acid/benzoyl protecting group combination (Leu-Bz-OH) as the most efficient for the reaction of Scheme 1, our work focused on this MPAA system. NMR studies of the interaction of Pd with the ligand in the presence of base revealed that deprotonation of the amino acid N–H occurred rapidly. The substrate **1** is also deprotonated in the presence of base even in the absence of catalyst. Intriguingly, we were unable to detect interactions between catalyst and substrate. Substrate titration showed no changes in the ^1H NMR spectrum. In addition, after mixing deutero **1-D** with Pd-Bz-Leu-OH and base in the DMSO/protio solvent mixture, or with protio **1** from the DMSO/deuteron solvent mixture, recovery of **1** was quantitative and no isotopic scrambling was observed, indicating both that substrate binding is very weak and that reversible C–H cleavage had not occurred (Scheme 2).

Further NMR studies revealed that interaction between the Pd salt and the ligand led to a rapid and quantitative *intramolecular* C–H activation process between the benzoyl protecting group of the bound ligand and Pd to form palladacycle **4**, as confirmed by ^1H and ^{13}C-DEPT-Q experiments. Palladacycle **4** represents a stable catalyst resting state, and we postulated that the lack of

Received: April 12, 2017
Published: June 12, 2017

DOI: 10.1021/jacs.7b03716
J. Am. Chem. Soc. 2017, 139, 9238–9245

Scheme 2. Substrate Interaction with Catalyst

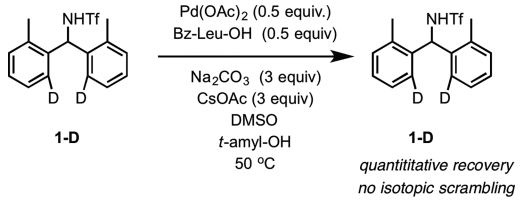

substrate binding and C−H activation as noted above could be a result of the inertness of **4**. Addition of I_2 may iodinate the benzoyl group to form the active catalyst prior to binding and reaction of substrate **1**. When the reaction in Scheme 1 was carried out using 2,6-difluorobenzoyl-protected leucine as ligand, where the *ortho* sites of the ligand are blocked, the reaction proceeds at the same rate and with the same enantioselectivity as the Bz-Leu-OH ligand. Thus, both catalyst systems are employed in these mechanistic studies.

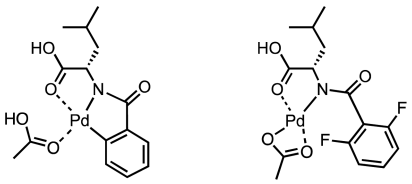

Reactions aimed at establishing catalyst robustness and concentration dependences of substrates **1** and **2** were carried out according to the "same excess" and "different excess" protocols of Reaction Progress Kinetic Analysis (RPKA),[5] with excess defined in eq 1.

$$[\text{excess}] = [\mathbf{2}]_0 - [\mathbf{1}]_0 \quad (1)$$

Figure 1 shows the kinetic profiles for experiments carried out using the "same excess" protocol. The time-adjusting curves, as

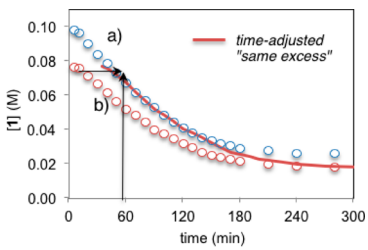

Figure 1. Kinetic profile for the C−H iodination reaction shown in Scheme 1 carried out using the "same excess" protocol with [excess] = 0.2 M. Both reactions with 0.01 M $Pd(OAc)_2$ and 0.02 M L-Bz-Leu-OH ligand with 3 equiv each Na_2CO_3 and CsOAc in DMSO/*t*-amyl alcohol at 50 °C. (a) $[\mathbf{1}]_0$ = 0.1 M; $[\mathbf{2}]_0$ = 0.3 M. (b) $[\mathbf{1}]_0$ = 0.08 M; $[\mathbf{2}]_0$ = 0.28 M.

marked by the arrows in Figure 1, allow for comparison of the kinetic profiles for the two reactions as they react under identical substrate concentrations onward from the point of intersection of the arrows. The fact that the profiles overlay indicates that reaction rate is not influenced by either the additional catalyst turnover or the presence of a higher concentration of product in the reaction vial for the case of run (a) as compared to run (b). This confirms that neither catalyst deactivation nor product inhibition is present in this robust catalyst system.

Figure 2 shows temporal product concentration profiles for "different excess" experiments. Figure 2a reveals that the rate

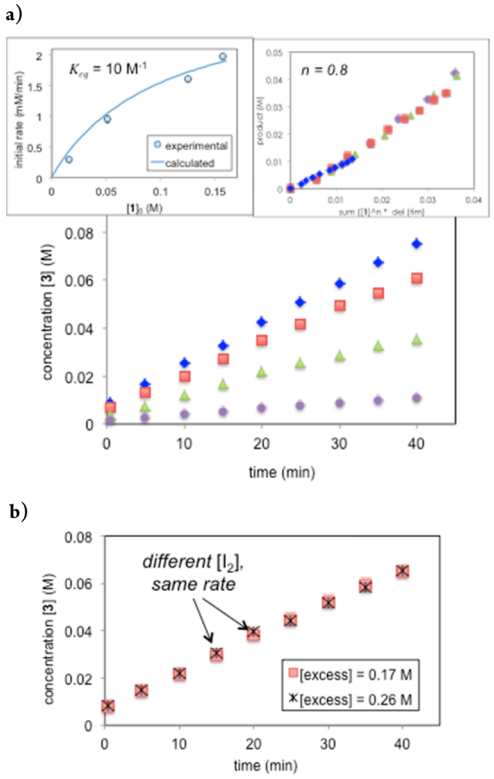

Figure 2. Different excess experiments to determine reaction orders in [**1**] and [**2**]. Catalyst/ligand system **5** with Pd:L = 2; all other conditions are given in Scheme 1. Top: concentration of product **3** plotted as a function of time with $[\mathbf{2}]_0$ = 0.4 M and $[\mathbf{1}]_0$ = 0.157 M (blue diamonds); $[\mathbf{1}]_0$ = 0.125 M (red squares); $[\mathbf{1}]_0$ = 0.051 M (green triangles); $[\mathbf{1}]_0$ = 0.016 M (purple circles). Inset left: initial rates vs $[\mathbf{1}]_0$ fit to saturation kinetics with K_{eq} = 10 M^{-1} Inset right: power law reaction order n = 0.8 calculated by the method of Burés (ref. 7). Bottom: concentration of product **3** plotted as a function of time with $[\mathbf{1}]_0$ = 0.13 M and $[\mathbf{2}]_0$ = 0.3 M ([excess] = 0.17 M, red squares); $[\mathbf{2}]_0$ = 0.39 M and ([excess] = 0.26 M, black crosses).

depends on [**1**] in a manner that is between zero and first order, which is characteristic of the saturation kinetics in [**1**]. The upper left inset plots the data as Michaelis−Menten kinetics, giving a binding equilibrium constant of $K_{eq} \approx 10$ M^{-1}. The right inset confirms this by plotting the data according to the Burés method[7] of determining the power law order in [**1**] to give n = 0.8. Figure 2b shows that the reaction exhibits zero-order kinetics in [**2**].

The initial rate data shown in the inset of Figure 2a are fit to the simple rate expression shown in eq 2. The catalyst concentration is lumped into k_{kin}, and the value of the binding constant K_{eq} = 10 M^{-1} suggests that at [**1**] = 0.1 M, ca. 50% of the catalyst is bound to **1**.

$$\text{rate} = \frac{k_{kin}[\mathbf{1}]}{1 + K_{eq}[\mathbf{1}]} \quad (2)$$

Reactions carried out using deuterated substrate **1** in global reactions gave lower rates, confirming a normal kinetic isotope effect (Figure 3). Fitting the initial rates as a function of [**1**-H] and [**1**-D] to the simple saturation kinetics model used for the data in Figure 3 revealed that the protio and deuterated substrates exhibit the same binding constant and differ in their

DOI: 10.1021/jacs.7b03716
J. Am. Chem. Soc. 2017, 139, 9238−9245

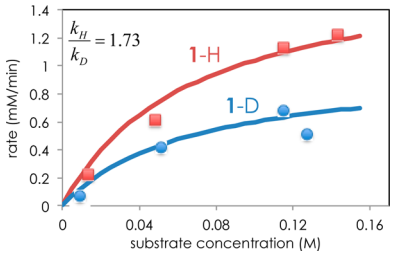

Figure 3. Reaction rate as a function of initial substrate concentration for the reaction in Scheme 1, carried out using catalyst/ligand system **5**, **1**-H, and **1**-D. $[\mathbf{2}]_0$ = 0.5 M; [Pd] = 0.025 M; [Pd]/[ligand] = 1:2; 3 equiv each Na_2CO_3 and CsOAc in DMSO/*t*-amyl alcohol at 50 °C.

elementary rate-determining step rate constant to give a value of k_H/k_D = 1.73. The magnitude of this value supports the kinetic observation that both the substrate binding and the subsequent C−H cleavage step contribute to the observed rate.

Reactions carried out using different concentrations of $Pd(OAc)_2$ showed that the reaction is first order in [Pd]. The base employed in these reactions appears to play a complex role, as the original studies found that a combination of two bases was most effective. The use of solid base suggests that mass-transfer limitations must be considered. Indeed, we found that the reaction rate increased with increased stirring speed. Grinding the Na_2CO_3 into fine particles prior to use in the reaction increased the rate further, at which point either low or high stirring speed gave the same rate (Figure 4). Kinetic profiles were

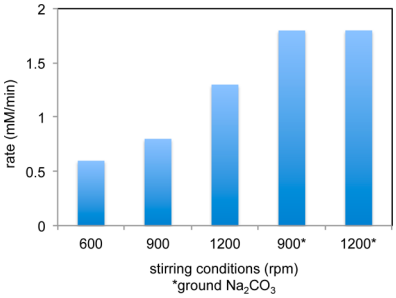

Figure 4. Reaction rates for the reaction in Scheme 1 carried out under identical conditions except for stirring speed and pregrinding of the Na_2CO_3 base. $[\mathbf{1}]_0$ = 0.1 M, $[\mathbf{2}]_0$ = 0.3 M, all other conditions as in Scheme 1.

linear in all cases. Both rapid stirring and pregrinding serve to increase the surface area for mass transfer between the solid base and the reaction solution.

A rate enhancement due to increased stirring/grinding coupled with the observation of overall zero-order kinetics is often attributed to that of a solid-solution mass-transfer step is rate-determining; however, the observation of first-order kinetics in [Pd] precludes this interpretation, because the catalyst should not be a factor in the solid-to-solution mass transfer of base, and the low solubility of the inorganic bases means that only a few percent conversion could be achieved from the quantity of base held in solution at saturation. A more likely rationalization of the stirring/grinding effect on rate is that the decrease in solid particle size results in an increase in the sparing solubility of the base due to the Gibbs−Thomson effect. Thus, rapid equilibrium in the solid-solution mass-transfer step maintains a constant solution concentration of base that is higher under aggressive stirring/grinding conditions. The further implication of these results is that the base is involved in a kinetically meaningful step in the catalytic cycle.

Reactions began to stall typically around 75−80% conversion of **1**, and the linear profiles indicative of overall zero-order kinetics in [**1**] and [**2**] altered at higher conversions as the reactions slowed. Because the same excess protocol had indicated a robust catalyst, we probed reasons other than catalyst deactivation or product inhibition for this failure to achieve complete conversion. We found that addition of further equivalents of I_2 allowed the reaction to progress further. Figure 5 shows the results of a reaction carried out initially with

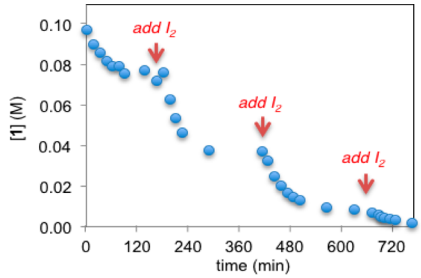

Figure 5. Kinetic profile for the C−H iodination reaction shown in Scheme 1, carried out with initial concentrations $[\mathbf{1}]_0 = [\mathbf{2}]_0$ = 0.1 M. An additional equivalent of **2** (0.1 M) was added three times as indicated in the figure.

equimolar concentrations of [**1**] and [**2**], with an additional equivalent of **2** added three further times until complete conversion of **1** was observed. The reaction cleanly afforded the product in 96% ee. This suggests that the lower yields and the stalling of the reaction is due to consumption of **2** in side reactions, whereas the catalyst maintains its activity over the entire course of the reaction. Consumption of I_2 was confirmed by the formation of green crystals in the crude reaction mixture at the end of the reaction which were identified by single -crystal X-ray analysis to be $Na_4(I_3)_3I(DMSO)_{15}$ (Figure 6). The requirement for multiple equivalents of I_2 to achieve high product yield in this reaction is rationalized by these results.

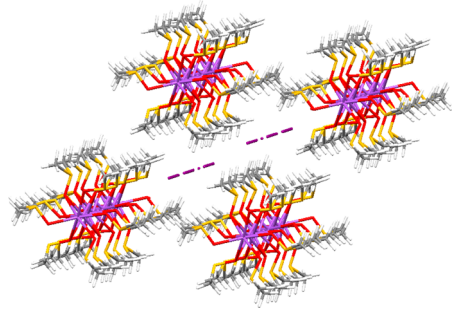

Figure 6. Unit cell of crystals formed in the crude reaction mixture at the end of the reaction in Scheme 1 with unit cell formula $Na_4(I_3)_3I(DMSO)_{15}$.

Activation parameters were determined by measuring reaction rate over a temperature range from 25 to 72 °C (Table 1, Figure 7). Remarkably, product ee was maintained above 96% ee over a range of nearly 50 °C, decreasing only to just below 95% ee at 84 °C. The reaction in the absence of ligand is 10-fold slower at 40 °C and exhibits a higher activation enthalpy and a lower activation entropy. Similar rates, activation parameters, and enantioselectivities were obtained in reactions using substituted

DOI: 10.1021/jacs.7b03716
J. Am. Chem. Soc. 2017, 139, 9238−9245

Table 1. Activation Parameters for the Reaction of Scheme 1

parameter	no ligand	Bz-Leu-OH
$\Delta H^{\ddagger}$ (kcal/mol)	25.2	16.8
$\Delta S^{\ddagger}$ (cal/mol/K)	3.6	−18

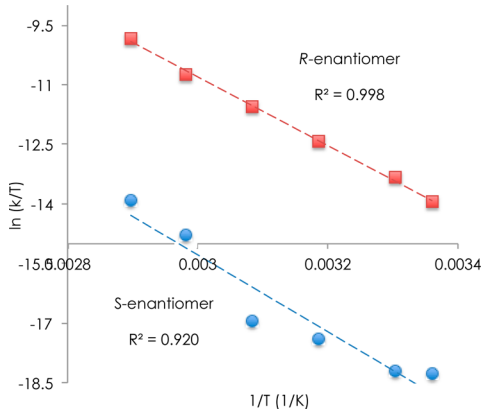

Figure 7. Eyring plot for each product enantiomer in the reaction of Scheme 1.

benzoyl protecting groups OMe-Bz-Leu-OH and CF_3-Leu-Bz-OH, indicating the lack of a strong electronic influence on the course of the reaction.

These observations appear to support a mechanism where moderately strong substrate−catalyst binding is followed by irreversible C−H activation and the addition of the reaction-coupling partner, in this case I_2, as has been documented in a number of different Pd(II)-catalyzed reactions involving these MPAA ligands. However, several additional features of the reaction invoke a more complex mechanistic picture. First, the mildness of the reaction conditions is in contrast with other cases where significantly higher temperatures are required to undergo C−H activation. Indeed, we found that much harsher conditions were required in our synthetic Pd-catalyzed reactions to produce the deuterated substrate for the KIE experiments.

Second, we found that we remain unable to detect substrate binding commensurate with the binding constant predicted by the reaction kinetics using catalyst **5** formed with the 2,6-F,F-Bz-Leu-OH ligand system. The kinetic fit of eq 2 predicts that **1** should ultimately partition to form Pd-**1** in an amount equal to the total [Pd] during reaction. However, a mass balance showed that recovered starting material was nearly quantitative, indicating much weaker binding between substrate **1** and catalyst **5** than is predicted from the reaction kinetics. Furthermore, we found that recovered **1**-D in interaction with **5** showed *no isotopic scrambling* in experiments mixing deuterated **1**-D and protic solvent, just as was found for the benzoyl ligand. These results confirm that neither reversible nor irreversible C−H cleavage occurs with catalyst **5** prior to addition of iodine. Intriguingly, given this apparent inertness of the substrate to C−H bond activation, the kinetic data clearly show that the reaction proceeds smoothly immediately upon addition of I_2 with either the original Pd-Leu-Bz-OH or catalyst **5**. This observed requirement for the presence of I_2 is all the more puzzling given that palladacycle **4** forms readily via C−H activation of the benzoyl protecting group of the ligand in the absence of I_2.

Further studies thus focused on probing the role of I_2 in triggering C−H activation in this system. The conventional mechanistic hypothesis for similar reactions obeying similar kinetics[6] involves substrate **1** binding to the Pd(II) center preceding addition of substrate **2**; an alternative hypothesis may be invoked that exhibits the same kinetic features. Positive-order kinetics in **1** and zero-order kinetics in **2** could result if **2** enters the cycle prior to **1** and forms the saturated catalyst resting state. Oxidative addition of iodine to the catalyst to form the species Pd(IV)-(**2**), occupying all of the Pd to form a completely saturated intermediate, would satisfy the observed zero-order kinetics in [**2**]. Substrate **1** binding reversibly to Pd(IV)-(**2**) followed by rate-determining C−H activation gives the observed saturation kinetics in [**1**] and normal deuterium isotope effect. If the C−H activation step proceeds via such a Pd(IV) species, with a role for I_2 in oxidizing Pd(II) to Pd(IV), a rationalization for the lack of C−H activation in the absence of iodine is provided.

Although reaction mechanisms proceeding through high oxidation state Pd(IV) have been proposed, and organo-palladium Pd(IV) complexes have been isolated,[8−10] their reactivity is less well-known than that of Pd(0) and Pd(II). In particular, oxidation of Pd is typically effected via hypervalent iodine reagents. Detailed studies of stoichiometric C−H activation via Pd(IV) complexes were carried out in the *para*-selective C−H arylation of monosubstituted arenes, where an [ArPd(IV)F] intermediate was invoked.[9c] The proposal of a Pd(IV) species in the current mechanistic scenario relies on the oxidizing capability of I_2. Cyclic voltammetry experiments carried out using catalyst **5** and increasing amounts of I_2 (Figure 8) reveal

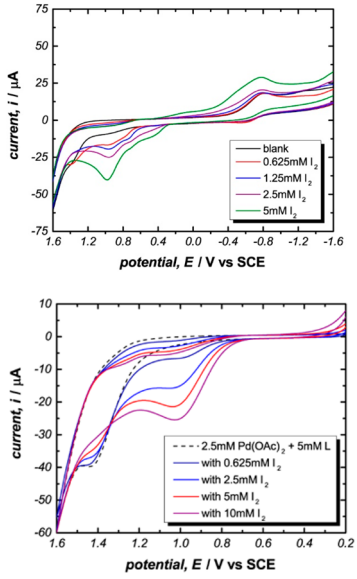

Figure 8. Cyclic voltammetry with variable concentration of I_2 alone (top) and with 1 mM $Pd(OAc)_2$ and 2.5 mM 2,6-F,F-Bz-Leu-OH. The peak at 0.95 V corresponds to oxidation of I_2. The disappearance of a peak at 1.4 V corresponds to Pd(II)/Pd(IV) oxidation.

an irreversible oxidation peak at 0.95 V (all potentials are given versus SCE) which corresponds to the oxidation of I_2 to I^+ and surface-adsorbed I.[11] A peak at 1.4 V corresponding to Pd(II)/Pd(IV) oxidation shows a decreasing concentration of Pd(II) as the concentration of I_2 increases. These experiments suggest that the 2,6-F,F-Bz-Leu-OH ligand provides for sufficient overlap in the **5** (Pd(II/IV)) and I_2 oxidation potentials to enable oxidative addition of I_2 directly to **5**. A more detailed description of the electrochemical results is provided in the Supporting Information and suggests the oxidative addition of I_2 to **5** is reversible and provides an equilibrium of Pd(II) and Pd(IV) that, under reaction concentrations of I_2, is shifted strongly toward Pd(IV).

DOI: 10.1021/jacs.7b03716
J. Am. Chem. Soc. 2017, 139, 9238−9245

Because substrate **1** is not involved in the Pd(IV)-forming process, this system appears to be different from those of previous studies where Pd(II)-mediated C−H cleavage forming a Pd(II) aryl or alkyl species precedes Pd oxidation and a second C−H cleavage by Pd(IV).

^{19}F NMR studies using catalyst **5** shed further light on this mechanistic proposal as shown in Figure 9. The leucine MPAA

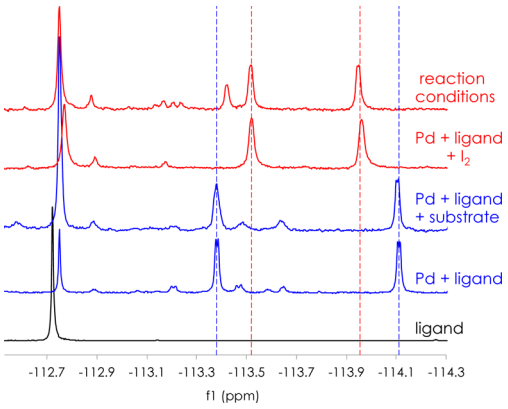

Figure 9. ^{19}F NMR studies of the role of iodine. (a) Free 2,6-F,F-Bz-Leu-OH ligand; (b) ligand + Pd; (c) ligand + Pd + substrate **1**; (d) ligand + Pd + I_2; (e) system with both substrate **1** and iodine **2** under reaction turnover. All spectra taken with Pd/L = 2:1 after heating to 50 °C in d_6-DMSO/*t*-amyl-OH with CsOAc.

ligand containing the 2,6-difluorobenzoyl protecting group gives a strong signal at −112.7 ppm (referenced to trifluorotoluene). Mixing the ligand with $Pd(OAc)_2$ produces a pair of peaks at −113.4 and 114.1 ppm (Figure 9, blue dashed lines). These peaks are unchanged when substrate **1** is added to the solution, supporting other evidence that the substrate does not interact strongly with the catalyst. However, when iodine is mixed with Pd and ligand, the peaks attributed to interaction between Pd and the ligand show a significant shift that is also observed under reaction conditions with both substrate **1** and I_2 (Figure 9, red dashed lines). These spectroscopic results demonstrate a change in the catalyst upon interaction with I_2 that is consistent with the proposal of oxidation to Pd(IV) from the electrochemical studies.

Further support for the requirement of Pd(IV) in such a mechanism comes from the inertness of a $Pd(II)I_2$ complex to react with amine **1**, as shown in Scheme 3. Although PdI_2 is a

Scheme 3. Reaction of PdI_2 and Amine 1 in the Absence and Presence of Molecular I_2

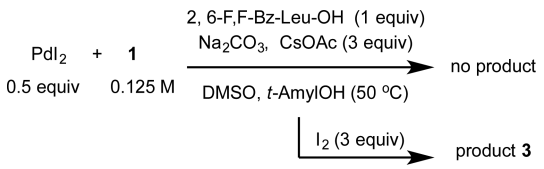

viable precatalyst in the reaction with **1** when I_2 is present, no product is formed under conditions of ($Pd(II)I_2$ + **1** + bases) prior to addition of molecular I_2.

A reaction mechanism accounting for all of these experimental observations is proposed in Scheme 4. Conversion of Pd(II) to Pd(IV) via oxidative addition of iodine to produce intermediate **A** precedes reversible substrate addition. Irreversible C−H activation of intermediate **C** is followed by transfer of iodine to

Scheme 4. Proposed Reaction Mechanism

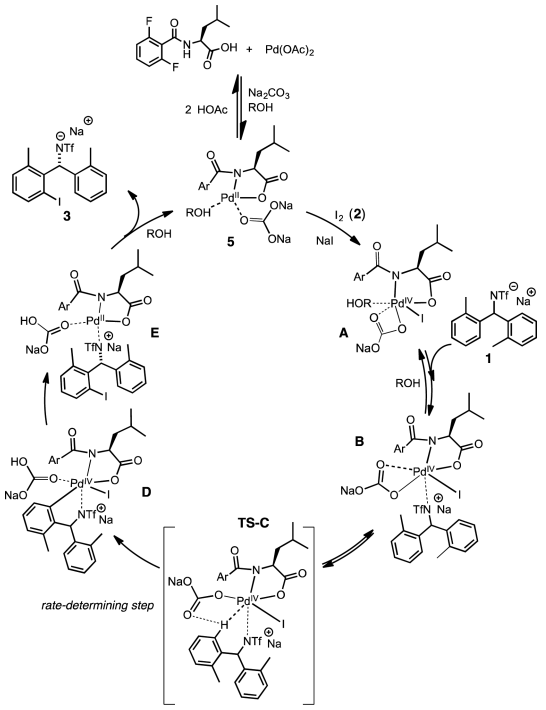

the palladacycle intermediate **D** and reductive elimination to regenerate catalyst **5**. The observed saturation kinetics in [**1**] along with the magnitude of the observed H/D KIE suggests that the resting state shifts between species **A** and **C** as a function of substrate concentration [**1**]. The cycle may be written as the elementary steps given in eqs 3−5, with the kinetically meaningful steps above the dashed line. Intermediates **D** and **E** are kinetically indistinguishable from **B**, as these species involve only internal transformations of the catalytic complexes.

$$\mathbf{A} + \mathbf{1} \overset{K_{eq}}{\rightleftarrows} \mathbf{B} \quad (3)$$

$$\mathbf{B} \overset{k_{rds}}{\longrightarrow} \mathbf{3} + \mathbf{5} \quad (4)$$

$$\mathbf{5} + \mathbf{2} \rightarrow \mathbf{A} \quad (5)$$

As noted above, this mechanism differs from previous proposals in which the substrate is involved in two C−H cleavage events, where Pd(IV) palladacycle formation is preceded by aryl or alkyl C−H cleavage by Pd(II). In the present case, experimental evidence suggests that the Pd(IV) species is formed without substrate involvement. Such a species represents a different class of precatalyst for C−H functionalization reactions as compared to the "double C−H cleavage" systems in which Pd(IV) has previously been implicated in the second step.

To probe this mechanistic hypothesis further, DFT calculations were carried out using L-Leu-Bz-OH as the MPAA ligand and a model Pd catalyst **I** (Figure 10) derived from experimental findings, composed of the dianionic MPAA ligand, one sodium carbonate molecule (required for the reaction), and one methanol molecule (model for *t*-amyl alcohol).[12]

The proposed first step of the catalytic cycle is oxidative addition of I_2 to the Pd(II)-center of the catalyst. As seen in Figure 11, this step of the reaction requires a 16.9 kcal/mol free energy barrier at transition state **TS-OA** and results in the oxidative addition product [MPAA]Pd(IV)I_2, **III**. It is exergonic

DOI: 10.1021/jacs.7b03716
J. Am. Chem. Soc. 2017, 139, 9238−9245

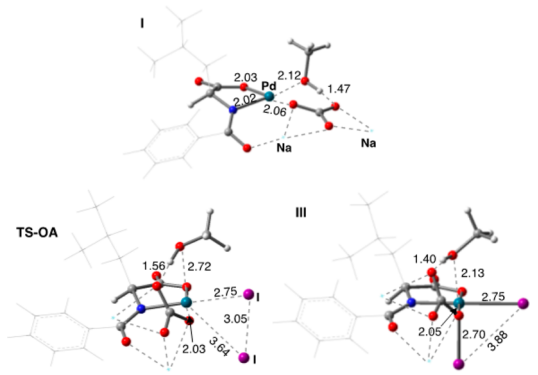

Figure 10. Important structural parameters of the model catalyst **I**, oxidative addition transition state **TS-OA**, and oxidative addition product [MPAA]Pd(IV)I_2, **III**, of the [MPAA]Pd(II) catalyst insertion into the I–I bond of I_2. Bond distances are in Å.

by 10.0 kcal/mol and is driven further by another 6.8 kcal/mol via extraction of an iodide from Pd(IV) by I_2 to form sodium triiodide and **IV**. Thus, overall the oxidative addition of I_2 to the Pd(II)-center of the [MPAA]/Pd(II) catalyst and subsequent triiodide formation, i.e. **I** → **IV**, is 16.8 kcal/mol exergonic. This result is in accordance with the experimental formation of $Na_4(I_3)_3I(DMSO)_{15}$ crystals and supports the observation that excess I_2 is required even for a reaction exhibiting zero-order kinetics in [I_2].

The next step of the reaction is the coordination of the substrate and the expulsion of MeOH to form intermediate **V**. This process is exergonic by 5.1 kcal/mol. The finding that substrate coordination is favorable is generally consistent with the experimental data presented above. Substrate C–H bond activation in complex **V**, required for C–H iodination, can occur through the following concerted-metalation-deprotonation (CMD) pathways:[13−15] (a) "internal-ligand-assisted", where the protecting group of the MPAA ligand is the base, or (b) "internal-carbonate-assisted", where the coordinated carbonate is the base. For Pd(II) reactions, the "internal-ligand-assisted" mechanism is widely studied and accepted,[16−20] but this pathway has not been investigated for Pd(IV) species.

We investigated both CMD pathways to explore the role of the MPAA ligand in C–H activation on Pd(IV) systems (see Figure 11). Calculations show that the "internal-ligand-assisted" C–H activation occurs through the **TS-CH-L** transition state with a free energy barrier of 26.4 kcal/mol, and the "internal-carbonate-assisted" C–H activation occurs through the transition state **TS-CH-C** with a free energy barrier of 23.3 kcal/mol (both calculated relative to intermediate **V**), demonstrating that the "internal-carbonate-assisted" C–H activation is kinetically favored. In addition, the "internal-carbonate-assisted" pathway is exergonic (**V** → **VII-C**, ΔG = −4.7 kcal/mol), whereas the "internal-ligand-assisted" pathway is endergonic (**V** → **VII-L**, ΔG = 4.9 kcal/mol). Thus, the "internal-carbonate-assisted" pathway is kinetically and thermodynamically preferred for C–H activation by Pd(IV)/MPAA systems, and the MPAA ligand does not directly participate in the rate-limiting C–H activation transition state as observed for the Pd(II)/MPAA systems. The lack of a Hammett effect of the ligand benzoyl group is in accordance with this finding.

Close examination of the transition state **TS-CH-C** shows that the "internal-carbonate-assisted" C–H activation occurs *trans* to the apical iodide ligand (see Figure 12), and isomerization is required to position the substrate aryl group and iodide in close vicinity for reductive elimination. This isomerization process, i.e. **VII-L** → **VIII**, requires only 5.0 kcal/mol free energy. In the resulting intermediate **VIII**, the bicarbonate ligand forms a hydrogen-bonding interaction with the carbonyl of the MPAA benzoyl protecting group.

The C–I reductive elimination occurs through the transition state **TS-RE** with a free energy barrier of 20.1 kcal/mol (relative

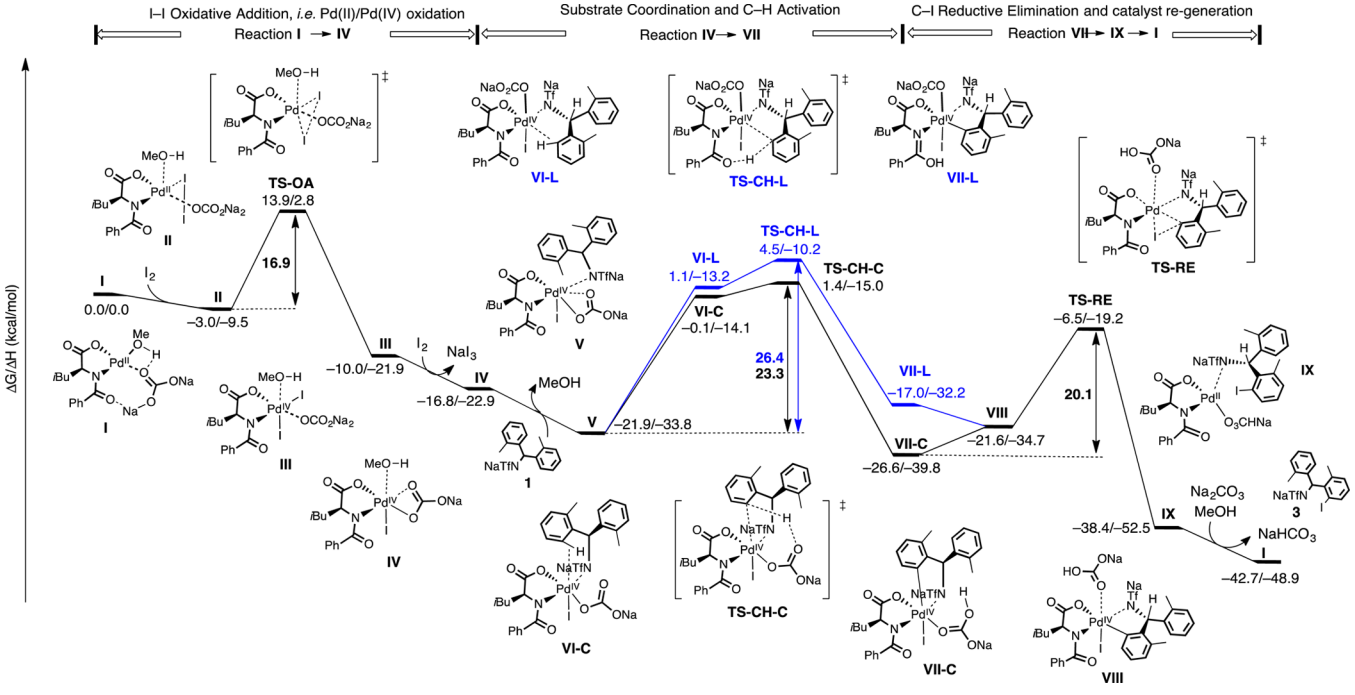

Figure 11. Calculated free-energy surface for the full catalytic cycle of C–H iodination by [MPAA]/Pd(II) catalyst with I_2. The "internal-ligand-assisted" pathway is shown in blue, and the "internal-carbonate-assisted" pathway is shown in black. Energies are reported as $\Delta G/\Delta H$ in kcal/mol.

DOI: 10.1021/jacs.7b03716
J. Am. Chem. Soc. 2017, 139, 9238−9245

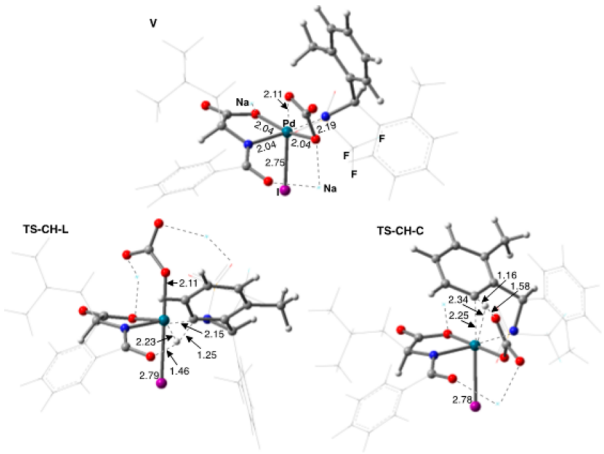

Figure 12. Important structural parameters for the [MPAA]/Pd(IV)-substrate intermediate **V** and "internal-ligand-assisted" and "internal-carbonate-assisted" C−H activation transition states **TS-CH-L** and **TS-CH-C**, respectively. Bond distances are in Å.

to **VII−C**). Formation of the reductive elimination product, **IX**, is exergonic by 11.8 kcal/mol relative to intermediate **VII−C**. Careful analysis of the geometries reveals that the bicarbonate ligand plays an important role in the reductive elimination step. First, the ligand dissociates from the Pd(IV) center, as evidenced by lengthening of the Pd−O distance upon going from **VIII** (Pd−O = 2.11 Å) to **TS-RE** (Pd−O = 2.29 Å). Dissociation of a ligand prior to reductive elimination on Pd(IV) has been described previously.[21,22] Next, bicarbonate participates in the transition state **TS-RE** to facilitate displacement of the aryl ligand as the C−I bond forms. As such, the Pd-carbonate bond is fully formed (Pd−O = 2.07 Å) in **IX**, as confirmed with an intrinsic reaction coordinate (IRC) calculation from **TS-RE** (see Figure 13). Subsequent deprotonation and product (**XI**) dissociation

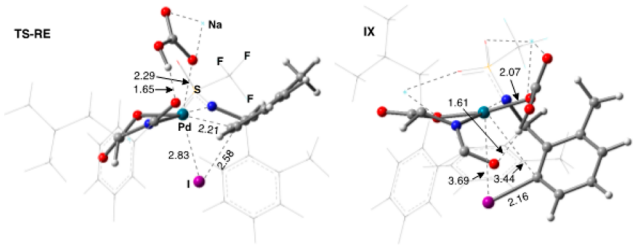

Figure 13. Important structural parameters for the C−I reductive elimination transition state **TS-RE** and product **IX**. Bond distances are in Å.

steps to regenerate catalyst **I** are exergonic, and the calculated reaction free energy for the entire reaction, i.e., **I** + **10** + 2 I_2 + Na_2CO_3 → **I** + **3** + NaI_3 + $NaHCO_3$, is ΔG = −42.7 kcal/mol.

The high enantioselectivity observed in this reaction is supported by transition-state calculations comparing **TS-CH-C** leading to the *R* vs the *S* product. As shown in Figure 14, the calculated energy difference between these transition states produces the correct stereoisomer, but it is much larger than that expected on the basis of the experimental ee value. This overestimation of the enantioselectivity suggests the possibility of additional complexity in the mechanism of asymmetric induction with the likelihood of several diastereomeric transition states that contribute to the observed enantioselectivity. Further

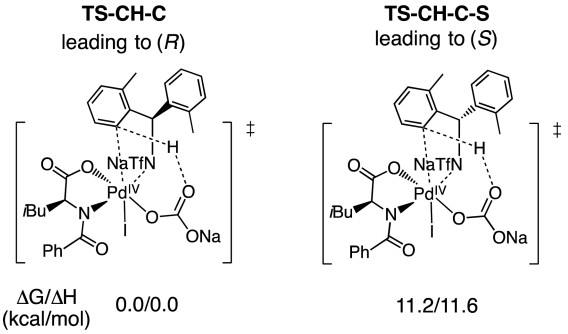

Figure 14. Transition-state energy ($\Delta G/\Delta H$ in kcal/mol) of the C−H cleavage step for the minor enantiomer compared to the major enantiomer (see Figure 11).

studies of enantioinduction including the relative insensitivity to temperature are ongoing.

These computational results are fully consistent with the experimental findings and indicate that I_2 oxidative addition to Pd(II) precedes rate-limiting C−H activation at Pd(IV). Strikingly, this proposed mechanism differs from the previously reported computational findings on the Pd(II)-catalyzed iodination by I_2 in systems both with[23] and without[24] MPAA ligands. It is important to note, however, that the substrates involved in the experimental and computational studies of iodination without MPAA ligands bear greater similarity to these ligands, both of which contain amide groups, than they do to the diarylmethylamine substrate **1** used in our work, which lacks the C═O functionality. Our finding of facile C−H functionalization to form palladacycle **4** between Pd(II) and the benzoyl group, coupled with the inertness of substrate **1** to this reaction with Pd(II) under mild conditions, suggests that the amide group plays an important role in the C−H activation process mediated by Pd(II).

CONCLUSIONS

An exhaustive mechanistic study of the enantioselective desymmetrization of diarylmethylamines catalyzed by Pd with MPAA ligands sheds new light on how the concept of weak coordination in C−H functionalization affords a rich variation in reaction pathways available to these systems. The mild reaction conditions in the present work steer the C−H activation step to a Pd(IV) species formed from oxidative addition of iodine to the Pd(II) catalyst. The reaction remains highly enantioselective over a wide temperature range and strikingly insensitive to the electronic characteristics of the ligand. DFT calculations provide insight into these findings. This work may lead to a better general understanding of the subtle variations in the reaction mechanisms for C−H functionalization reactions that may be extant for this ligand class depending on substrate, amino acid ligand and protecting group, and reaction conditions.

ASSOCIATED CONTENT

Supporting Information

The Supporting Information is available free of charge on the ACS Publications website at DOI: 10.1021/jacs.7b03716.

Details of kinetic and mechanistic experiments; computational details; optimized structures along the full catalytic cycle for C−H iodination by [MPAA]Pd(II) catalyst with I_2; calculated energies for coordination of the substrate to model Pd(II) and Pd(IV) complexes on the reaction pathway; computed energies in hartree for all reported

DOI: 10.1021/jacs.7b03716
J. Am. Chem. Soc. 2017, 139, 9238−9245

structures; Cartesian (xyz) coordinates of all reported structures; (PDF)
X-ray data (CIF)

AUTHOR INFORMATION

Corresponding Author

*Blackmond@scripps.edu

ORCID

Brandon E. Haines: 0000-0002-5013-8396
Djamaladdin G. Musaev: 0000-0003-1160-6131
Jin-Quan Yu: 0000-0003-3560-5774
Donna G. Blackmond: 0000-0001-9829-8375

Notes

The authors declare no competing financial interest.

ACKNOWLEDGMENTS

This work was supported by the National Science Foundation under the CCI Center for Selective C−H Functionalization (CHE-1205646). D.G.M. and B.E.H. gratefully acknowledge NSF MRI-R2 grant (CHE-0958205 for D.G.M.) and the use of the resources of the Cherry Emerson Center for Scientific Computation. Helpful advice on NMR spectroscopy from D. Huang and L. Paternack (TSRI) is acknowledged. Curtis Moore and Arnold Rheinhold (UCSD) and Oana Luca (TSRI) are acknowledged for the crystallography studies.

REFERENCES

(1) Engle, K. E.; Mei, T. S.; Wasa, M.; Yu, J.-Q. *Acc. Chem. Res.* **2012**, *45*, 788−802.
(2) Chu, L.; Wang, Y.-C.; Moore, C. E.; Rheingold, A. L.; Yu, J.-Q. *J. Am. Chem. Soc.* **2013**, *135*, 16344−16347.
(3) Chu, L.; Xiao, K.-J.; Yu, J.-Q. *Science* **2014**, *346*, 451−455.
(4) Wang, X.-C.; Hu, Y.; Bonacorsi, S.; Hong, Y.; Burrell, R.; Yu, J.-Q. *J. Am. Chem. Soc.* **2013**, *135*, 10326−10329.
(5) (a) Blackmond, D. G. *Angew. Chem., Int. Ed.* **2005**, *44*, 4302. (b) Mathew, J. S.; Klussmann, M.; Iwamura, H.; Valera, F.; Futran, A.; Emanuelsson, E. A. C.; Blackmond, D. G. *J. Org. Chem.* **2006**, *71*, 4711.
(6) Baxter, R. D.; Sale, D.; Engle, K. M.; Yu, J.-Q.; Blackmond, D. G. *J. Am. Chem. Soc.* **2012**, *134*, 4600.
(7) Bures, J. *Angew. Chem., Int. Ed.* **2016**, *55*, 16084.
(8) Xu, L.-M.; Li, B.-J.; Yang, Z.; Shi, Z.-J. *Chem. Soc. Rev.* **2010**, *39*, 712−733.
(9) (a) Hull, K. L.; Lanni, E. L.; Sanford, M. S. *J. Am. Chem. Soc.* **2006**, *128*, 14047−14049. (b) Whitfield, S. R.; Sanford, M. S. *J. Am. Chem. Soc.* **2007**, *129*, 15142. (c) Racowski, J. M.; Ball, N. D.; Sanford, M. S. *J. Am. Chem. Soc.* **2011**, *133*, 18022−18025.
(10) (a) Rosewall, C. F.; Sibbald, P. A.; Liskin, D. V.; Michael, F. E. *J. Am. Chem. Soc.* **2009**, *131*, 9488−9489. (b) Sibbald, P. A.; Rosewall, C. F.; Swartz, R. D.; Michael, F. E. *J. Am. Chem. Soc.* **2009**, *131*, 15945−15951.
(11) Geissler, W.; Nitzsche, R.; Landsberg, R. *Electrochim. Acta* **1966**, *11*, 389−400.
(12) DFT calculations were performed at the [B3LYP-D3/6-311+g(2d,p) and SDD for Pd, I]//[B3LYP-D3/6-31g(d,p) and Lanl2dz for Pd, I] level of theory. Bulk solvent effects were included in all calculations with an implicit solvation model (IEF-PCM) for methanol. See SI for full computational details.
(13) Biswas, B.; Sugimoto, M.; Sakaki, S. *Organometallics* **2000**, *19*, 3895−3908.
(14) Davies, D. L.; Donald, S. M. A.; Macgregor, S. A. *J. Am. Chem. Soc.* **2005**, *127*, 13754−13755.
(15) Gorelsky, S. I.; Lapointe, D.; Fagnou, K. *J. Am. Chem. Soc.* **2008**, *130*, 10848−10849.
(16) Cheng, G. J.; Chen, P.; Sun, T. Y.; Zhang, X. H.; Yu, J. Q.; Wu, Y. D. *Chem. - Eur. J.* **2015**, *21*, 11180−11188.
(17) Cheng, G. J.; Yang, Y. F.; Liu, P.; Chen, P.; Sun, T. Y.; Li, G.; Zhang, X. H.; Houk, K. N.; Yu, J. Q.; Wu, Y. D. *J. Am. Chem. Soc.* **2014**, *136*, 894−897.
(18) Haines, B. E.; Musaev, D. G. *ACS Catal.* **2015**, *5*, 830−840.
(19) Musaev, D. G.; Figg, T. M.; Kaledin, A. L. *Chem. Soc. Rev.* **2014**, *43*, 5009−5031.
(20) Engle, K. M. *Pure Appl. Chem.* **2016**, *88*, 119−138.
(21) Camasso, N. M.; Perez-Temprano, M. H.; Sanford, M. S. *J. Am. Chem. Soc.* **2014**, *136*, 12771−12775.
(22) Furuya, T.; Benitez, D.; Tkatchouk, E.; Strom, A. E.; Tang, P. P.; Goddard, W. A.; Ritter, T. *J. Am. Chem. Soc.* **2010**, *132*, 3793−3807.
(23) Zhou, M. J.; Yang, T. L.; Dang, L. *J. Org. Chem.* **2016**, *81*, 1006−1020.
(24) Haines, B. E.; Xu, H. Y.; Verma, P.; Wang, X.; Yu, J. Q.; Musaev, D. G. *J. Am. Chem. Soc.* **2015**, *137*, 9022−9031.

DOI: 10.1021/jacs.7b03716
J. Am. Chem. Soc. 2017, 139, 9238−9245